Published in final edited form as:

Cell Rep. 2018 June 12; 23(11): 3197–3208. doi:10.1016/j.celrep.2018.05.037.

Corticostriatal Transmission Is Selectively Enhanced in Striatonigral Neurons with Postnatal Loss of *Tsc1*

Katelyn N. Benthall[1], **Stacie L. Ong**[1], and **Helen S. Bateup**[1,2,3,*]

[1]Department of Molecular and Cell Biology, University of California, Berkeley, Berkeley, CA 94720, USA

[2]Helen Wills Neuroscience Institute, University of California, Berkeley, Berkeley, CA 94720, USA

SUMMARY

mTORC1 is a central signaling hub that integrates intra- and extracellular signals to regulate a variety of cellular metabolic processes. Mutations in regulators of mTORC1 lead to neurodevelopmental disorders associated with autism, which is characterized by repetitive, inflexible behaviors. These behaviors may result from alterations in striatal circuits that control motor learning and habit formation. However, the consequences of mTORC1 dysregulation on striatal neuron function are largely unknown. To investigate this, we deleted the mTORC1 negative regulator *Tsc1* from identified striatonigral and striatopallidal neurons and examined how cell-autonomous upregulation of mTORC1 activity affects their morphology and physiology. We find that loss of Tsc1 increases the excitability of striatonigral, but not striatopallidal, neurons and selectively enhances corticostriatal synaptic transmission. These findings highlight the critical role of mTORC1 in regulating striatal activity in a cell type- and input-specific manner, with implications for striatonigral pathway dysfunction in neuropsychiatric disease.

Graphical abstract

In Brief Benthall et al. demonstrate that postnatal deletion of the autism-risk gene *Tsc1* causes cell-type-specific changes in striatal neuron morphology and physiology. They find that Tsc1 KO striatonigral, but not striatopallidal, neurons are hyperexcitable and have enhanced cortical excitatory synaptic transmission in the absence of changes to inhibition.

*Correspondence: bateup@berkeley.edu, https://doi.org/10.1016/j.celrep.2018.05.037.

[3]Lead Contact

SUPPLEMENTAL INFORMATION

Supplemental Information includes Supplemental Experimental Procedures, two figures, and four tables and can be found with this article online at https://doi.org/10.1016/j.celrep.2018.05.037.

AUTHOR CONTRIBUTIONS

Conceptualization, H.S.B.; Methodology, K.N.B. and S.L.O.; Formal Analysis, K.N.B. and S.L.O.; Investigation, K.N.B. and S.L.O.; Writing – Original Draft, K.N.B.; Writing – Review & Editing, K.N.B. and H.S.B.; Visualization, K.N.B. and H.S.B.; Supervision, K.N.B. and H.S.B.; Funding Acquisition, H.S.B.

DECLARATION OF INTERESTS

The authors declare no competing interests.

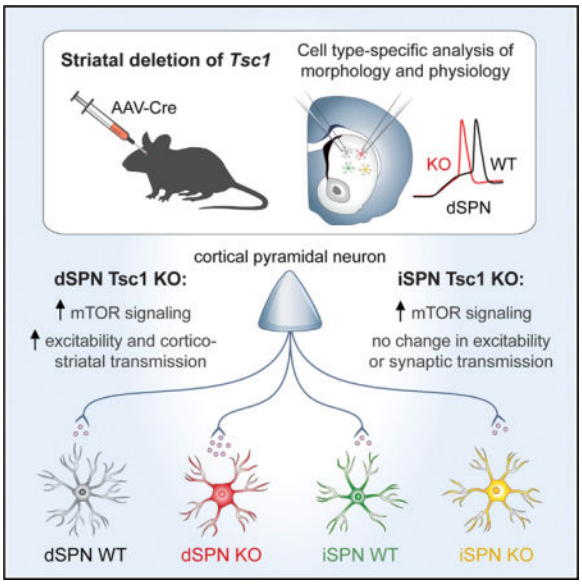

INTRODUCTION

The mechanistic target of rapamycin (mTOR) signaling pathway is a central coordinator of cell growth and metabolism. Activation of mTOR complex 1 (mTORC1) signals anabolic processes via stimulation of protein synthesis, organelle biogenesis, and suppression of autophagy (Saxton and Sabatini, 2017). In the nervous system, mTORC1 controls neuronal output by regulating intrinsic excitability, synaptic transmission, and long-term synaptic plasticity in a cell-type-specific manner (Bateup et al., 2011, 2013; Tavazoie et al., 2005; Ehninger et al., 2008; Tsai et al., 2012; Normand et al., 2013; Yang et al., 2012). Tight regulation of mTOR signaling is essential, as its dysregulation is associated with a variety of neurological and psychiatric disorders (Costa-Mattioli and Monteggia, 2013; Lipton and Sahin, 2014). In particular, several neurodevelopmental disorders are caused by mutations in regulators of mTORC1. One of these, tuberous sclerosis complex (TSC), is caused by mutations in the *TSC1* or *TSC2* genes, which encode components of a protein complex that negatively regulates mTORC1 signaling (Crino et al., 2006). Loss of the TSC1/2 complex causes deregulated and constitutively active mTORC1, leading to a syndrome characterized by high rates of epilepsy, intellectual disability, and autism spectrum disorder (ASD) (Crino, 2013; Curatolo et al., 2015). How dysregulated mTORC1 signaling causes these diverse phenotypes is not well understood, but current hypotheses suggest that mTOR-dependent alterations in neuronal excitability and synaptic balance cause aberrant circuit development and function.

The specific physiological phenotypes associated with mTORC1 deregulation are cell type dependent, indicating that the cellular context plays an important role in determining the outcome of mTOR pathway mutations. For example, in the hippocampus, loss of Tsc1 impairs mGluR-dependent long-term depression and inhibitory synapse function, leading to network hyperactivity (Bateup et al., 2011, 2013; Ehninger et al., 2008; Weston et al., 2014). Mosaic deletion of *Tsc1* from thalamic neurons alters their passive membrane properties and

action potential kinetics in an age-dependent manner (Normand et al., 2013). Loss of Tsc1 in the hypothalamus causes intrinsic hypoexcitability of Pomc- but not Agrp-expressing neurons (Yang et al., 2012). In the cerebellum, deletion of *Tsc1* from Purkinje cells causes hypoexcitability and cell death, with no major effects on synaptic transmission (Tsai et al., 2012). This diversity of responses to mTORC1 activation highlights the need to examine the consequences of mTOR signaling alterations in a cell-type- and circuit-specific manner.

Emerging evidence suggests that changes in the activity of striatal neurons may underlie the repetitive, inflexible behaviors associated with ASD (Fuccillo, 2016). The striatum is the main input structure of the basal ganglia, a group of subcortical nuclei that control action selection, motor learning, and habit formation (Graybiel, 2005; Graybiel and Grafton, 2015). The principal cells of the striatum are GABAergic spiny projection neurons (SPNs) that can be divided into two subtypes: striatonigral neurons of the direct pathway (dSPNs) that express type 1 dopamine receptors (D1) and striatopallidal neurons of the indirect pathway (iSPNs) that express type 2 dopamine receptors (D2) (Gerfen and Surmeier, 2011). Striatal SPNs are driven by glutamatergic inputs from the cortex and thalamus and project to distinct basal ganglia nuclei on the basis of their subtype (Smith et al., 1998; Kreitzer, 2009). Coordinated activity among ensembles of dSPNs and iSPNs determines basal ganglia output such that appropriate actions are selected while competing actions are suppressed (Mink, 2003; Klaus et al., 2017). Disruptions in the balance of activity between dSPNs and iSPNs result in altered motor behaviors in a variety of neurological and psychiatric disorders (Gunaydin and Kreitzer, 2016; Kravitz et al., 2010; Bateup et al., 2010), including mouse models of ASD (Fuccillo, 2016). Despite the known involvement of mTOR signaling in ASD, both in TSC and in other forms of autism (Curatolo et al., 2010; Davis et al., 2015; Huber et al., 2015; Subramanian et al., 2015), the consequences of mTORC1 deregulation on striatal activity are largely unknown.

To elucidate the impact of TSC-mTOR signaling on striatal neuron function, we conditionally deleted *Tsc1* from a subset of striatonigral and striatopallidal neurons and examined their morphological and physiological properties. We found that postnatal deletion of *Tsc1* resulted in a cell-type-specific increase in dSPN excitability, mediated by changes in passive membrane properties, potassium channels, and dendritic morphology. In addition, loss of Tsc1 caused a selective enhancement of corticostriatal synaptic inputs onto dSPNs, with no major changes to thalamic or inhibitory synaptic transmission. These results indicate that increased excitability of dSPNs is a primary effect of deregulated TSC-mTOR signaling, which may lead to striatal circuit dysfunction by altering the balance of activity between dSPNs and iSPNs.

RESULTS

Upregulation of mTORC1 and Somatic Hypertrophy in SPNs with *Tsc1* Deletion

To define the consequences of mTORC1 activation on striatal neuron function, we used a viral strategy to delete *Tsc1* from a subset of neurons in the dorsolateral striatum. We injected dilute AAV5-Cre-mCherry or AAV5-Cre-GFP virus into the striatum of juvenile *Tsc1*$^{fl/fl}$*;D2-GFP* or *Tsc1*$^{fl/fl}$*;D1-tdTomato* mice, respectively, and performed experiments 11–15 days later. This paradigm enabled fluorescence-based identification and subsequent

comparison of control (wild-type, WT) and *Tsc1* knockout (Tsc1 KO) dSPNs and iSPNs in the same striatal slice (Figures 1A–1F and S1A–S1F). With this approach, we could isolate the cell-autonomous effects of mTORC1 deregulation, independent of developmental or compensatory alterations, as ~25% of cells in the injection area express Cre recombinase and the injection site is restricted to dorsal striatum (Figures S1G and S1H). In striatal sections, immunostaining with a phospho-antibody against the downstream mTORC1 pathway target S6 (p-S6, Ser240/244) revealed an increase in mTORC1 activity in Tsc1 KO dSPNs and iSPNs compared with neighboring uninfected neurons (Figures 1B–1G and S1B–S1F). This confirms that Tsc1/2 complex function is impaired and mTORC1 is cell autonomously upregulated in Cre-expressing neurons.

A common phenotype associated with upregulation of mTORC1 signaling is somatic hypertrophy, which likely results from overactivation of mTORC1-regulated growth processes (Bateup et al., 2011; Meikle et al., 2007; Normand et al., 2013; Tavazoie et al., 2005; Tsai et al., 2012). To investigate if striatal neurons display this phenotype, we reconstructed somata in three dimensions from histology sections and measured soma volume using the NeuN signal. Tsc1 KO dSPNs and iSPNs had significantly increased soma volume compared with controls (Figure 1H), consistent with previous findings. A significant difference in soma volume was also detected between dSPN and iSPN control cells, with dSPNs having slightly larger cell bodies (Figure 1H). We confirmed the effects of Tsc1 loss on soma size in a separate analysis of iSPNs in *Tsc1*$^{fl/fl}$*;D2-GFP* mice using the GFP signal to measure soma volume (iSPN WT mean = 255.5 ± 2.4 μm^3, iSPN KO mean = 291.8 ± 2.7 μm^3, $p < 0.0001$, Kolmogorov-Smirnov [K-S] test).

Intrinsic Excitability Is Selectively Enhanced in Tsc1 KO dSPNs

To understand how loss of Tsc1 affects striatal neuron function, we first investigated how intrinsic excitability is affected by *Tsc1* deletion. We performed whole-cell current-clamp recordings of identified WT and Tsc1 KO dSPNs and iSPNs in striatal slices from *Tsc1*$^{fl/fl}$*;D2-GFP* mice injected with AAV5-Cre-mCherry. Recordings for this and all subsequent experiments were performed from cells in the dorsolateral striatum. We injected a depolarizing current step (75–400 pA, 500 ms) and measured firing frequency as a function of current step amplitude. We observed the previously reported difference in frequency-current relationship between dSPN and iSPN control cells (Gertler et al., 2008), with iSPNs having significantly increased intrinsic excitability (Figures 2A and 2B; Table S1). Interestingly, we found a significant difference between dSPN WT and Tsc1 KO neurons, with dSPN KO cells firing at a higher rate in response to current injection (Figures 2A and 2B; Table S1). Notably, no significant difference in frequency-current relationship was found between iSPN WT and KO neurons (Figures 2A and 2B).

As another measure of excitability, we determined the rheobase, the minimum current required to elicit a single action potential, by applying a series of depolarizing current steps in 10 pA increments (75–300 pA, 500 ms). Rheobase was significantly decreased in dSPN Tsc1 KO cells compared with controls, with no changes in Tsc1 KO iSPNs (Figure 2C). Lower rheobase current in Tsc1 KO dSPNs is consistent with increased excitability, as it indicates that less depolarization is required to evoke action potential firing. Consistent with

the enhanced excitability of Tsc1 KO dSPNs, membrane resistance was significantly increased and capacitance was significantly decreased compared with controls (Figures S1I and S1J). We found no differences in the passive properties of iSPN WT and Tsc1 KO cells (Figures S1I–S1K). Together these findings show that postnatal loss of Tsc1 selectively enhances the intrinsic excitability of dSPNs.

In addition to passive membrane properties, inwardly rectifying potassium channels (Kirs) are important for setting the membrane excitability of SPNs (Gertler et al., 2008; Kreitzer, 2009; Shen et al., 2007). Previous work has shown that the excitability difference between SPN subtypes is associated with greater Kir current in dSPNs compared with iSPNs (Gertler et al., 2008). We therefore tested whether loss of Tsc1 affects Kir currents in striatal neurons. To activate potassium conductances, we applied a series of voltage steps (−150 to −60 mV, 500 ms) in 10 mV increments in whole-cell voltage-clamp recordings. The predominant current in SPNs at hyperpolarized membrane potentials is through Kir channels; however, there is some contribution of leak conductances. To isolate Kir current, we blocked Kir channels with 1 mM CsCl and repeated the voltage step protocol. Kir currents were isolated from the Cs-insensitive leak conductances using digital subtraction (Figure 2D) (Cazorla et al., 2012). As previously reported (Gertler et al, 2008), Kir current was significantly larger in dSPN than iSPN control cells (Figures 2D and 2E; Table S1). Consistent with the enhanced intrinsic excitability of dSPN Tsc1 KO neurons, there was a significant decrease in Kir current in dSPN Tsc1 KO cells compared with controls (Figures 2D and 2E; Table S1). We also observed a small enhancement of Kir current at the most hyperpolarized membrane potential in Tsc1 KO iSPNs compared with WT iSPNs (Figures 2D and 2E; Table S1).

Dendritic Complexity Is Reduced in Tsc1 KO dSPNs

The degree of dendritic arborization strongly influences the membrane excitability of SPNs (Gertler et al., 2008). We therefore examined how dendritic morphology is affected by loss of Tsc1, as this could contribute to changes in excitability. Neurobiotin was dialyzed into cells during whole-cell recordings and visualized in fixed tissue sections using fluorophore-conjugated avidin. Dendritic arbors were reconstructed in three dimensions (Figure 3A), and arborization was quantified by Sholl analysis. We found that the dendritic complexity of dSPN Tsc1 KO cells was significantly decreased compared with that of controls, while iSPN Tsc1 KO and control cells had a similar Sholl profile (Figures 3A–3C; Table S1). Consistent with these findings, total dendrite length was significantly decreased in dSPN Tsc1 KO cells, resulting from decreased dendrite branching (Figures 3D–3F; Tables S2 and S3). Similar to prior studies (Gertler et al., 2008), we found that dSPN control cells had significantly greater dendritic complexity, total dendritic length, number of primary dendrites, and branchpoints compared with iSPNs (Figures 3D–3F; Tables S2 and S3). Taken together, these results demonstrate that acute loss of Tsc1 and cell autonomous activation of mTORC1 signaling affects the intrinsic properties of dSPNs in multiple ways, with the net effect of enhancing their excitability.

Loss of Tsc1 Does Not Affect Synaptic Inhibition onto SPNs

mTORC1 is an important regulator of synaptic properties in several neuron types, and changes in synaptic function are thought to underlie mTOR-related disorders (Hoeffer and

Klann, 2010). For example, in hippocampal neurons, loss of Tsc1 and activation of mTORC1 increases the excitatory/inhibitory synaptic ratio because of a strong decrease in inhibitory synapse function (Bateup et al., 2013). To determine how loss of Tsc1 affects inhibition onto striatal neurons, we examined baseline inhibitory transmission by recording miniature inhibitory postsynaptic currents (mIPSCs) in *Tsc1*$^{fl/fl}$*;D2-GFP* mice injected with AAV5-Cre-mCherry (Figure 4A). No differences in average mIPSC amplitude or frequency were observed with *Tsc1* deletion in either SPN type (Figures 4B–4E). To determine whether loss of Tsc1 affects evoked inhibitory synaptic transmission, we recorded electrically evoked IPSCs in simultaneously recorded pairs of WT and Tsc1 KO dSPNs or iSPNs. We found no difference in IPSC amplitude between Tsc1 KO SPNs and controls (Figures 4F–4H). Because SPNs receive many sources of inhibition (Tepper et al., 2010) that could be differentially affected by *Tsc1* deletion, we assayed inhibition in an input-specific manner. Fast-spiking parvalbumin-expressing interneurons (PV cells) control the activity of SPNs via feedforward inhibition (Koós and Tepper, 1999), and their dysfunction has been implicated in striatal-based disorders (Gittis and Kreitzer, 2012). To selectively activate inputs from PV cells, we bred the *Tsc1*$^{fl/fl}$*;D1-tdTomato* mice to mice expressing optimized FLP recombinase (FlpO) under the *Pvalb* (parvalbumin) promoter (*Pvalb-2A-FlpO-D*; Madisen et al., 2010). Juvenile mice were injected with AAV5-fDIO-ChR2-EYFP (Fenno et al., 2014) and AAV5-Cre-GFP to selectively express channelrhodopsin (ChR2) in PV cells and delete *Tsc1* from a subset of striatal neurons, respectively. We performed simultaneous paired recordings of Tsc1 KO and control dSPNs and activated PV cell inputs using full-field optical stimulation (Figures 4I and 4J). We found no difference in the amplitude of optically evoked IPSCs (oIPSCs) between Tsc1 KO and control dSPNs (Figure 4K). Together these results show that acute, postnatal loss of Tsc1 does not strongly affect inhibitory synaptic function in SPNs.

Synaptic Excitation Is Selectively Increased in Tsc1 KO dSPNs

SPNs exhibit low baseline firing activity but are strongly driven by glutamatergic inputs (Wilson and Kawaguchi, 1996). To test whether loss of Tsc1 affects excitatory synaptic transmission in SPNs, we recorded miniature excitatory postsynaptic currents (mEPSCs) in *Tsc1*$^{fl/fl}$*;D2-GFP* mice injected with AAV5-Cre-mCherry (Figure 5A). No difference in average mEPSC amplitude was found between conditions. However, the frequency of mEPSCs was selectively increased in dSPN Tsc1 KO cells compared with controls (Figures 5B–5E). We verified that these results were not specific to the *D2-GFP* transgenic mouse line by repeating this experiment in *Tsc1*$^{fl/fl}$*;D1-tdTomato* mice. Again, we found a selective increase in mEPSC frequency in Tsc1 KO dSPNs but not iSPNs (Figures S2A–S2C). Enhanced mEPSC frequency can result from either an increase in the number of excitatory synapses or an increase in presynaptic release probability. To test whether synapse number was affected by Tsc1 loss, we measured the density of dendritic spines, the sites of excitatory synapses onto SPNs, and found no difference between control and Tsc1 KO dSPNs (Figures S2D and S2E).

To determine whether loss of Tsc1 affects evoked excitatory synaptic transmission, we recorded electrically evoked EPSCs in simultaneously recorded pairs of WT and Tsc1 KO dSPNs or iSPNs (Figure 5F). Consistent with the mEPSC experiments, dSPN Tsc1 KO cells

had significantly larger EPSCs than controls (Figure 5G). No difference in EPSC amplitude was observed between iSPN WT and Tsc1 KO cells (Figure 5H). To test whether the increased EPSC amplitude and mEPSC frequency in Tsc1 KO dSPNs were due to changes in presynaptic release probability, we performed paired-pulse experiments and found a decrease in paired-pulse ratio in dSPN Tsc1 KO cells compared with controls, indicating enhanced presynaptic release probability (Figures 5I and 5J). No difference in the paired-pulse ratio was observed between iSPN WT and Tsc1 KO cells (Figures 5I and 5K). These results demonstrate that loss of Tsc1 selectively alters excitatory/inhibitory synaptic balance in dSPNs via a strengthening of glutamatergic inputs without a concurrent change to GABAergic transmission.

Selective Enhancement of Corticostriatal Transmission onto Tsc1 KO dSPNs

The major excitatory inputs to the striatum arise from the cortex and thalamus (Kreitzer and Malenka, 2008), either or both of which could mediate the increased excitatory drive observed in Tsc1 KO dSPNs. Determining the source of the enhanced excitation is important for understanding its functional consequences, as thalamostriatal terminals are involved in attention and switching between tasks, whereas corticostriatal synapses are implicated in motor learning and habit formation (Graybiel, 2005; Graybiel and Grafton, 2015; Smith et al., 2011). To activate specific glutamatergic inputs, we expressed ChR2 (AAV5-ChR2-mCherry) in either the thalamus or the cortex of *Tsc1*$^{fl/fl}$*; D1-tdTomato* mice injected with AAV5-Cre-GFP into the striatum (Figures 6A and 6D). We measured input-specific synaptic responses in simultaneously recorded pairs of WT and Tsc1 KO dSPNs. In response to optical stimulation of thalamostriatal terminals, we found no difference in the amplitude of subthreshold excitatory postsynaptic potentials (oEPSPs) between control and Tsc1 KO dSPNs (Figures 6B and 6C). However, stimulation of cortical terminals resulted in significantly greater oEPSP amplitude in dSPN Tsc1 KO cells compared with WT, indicating that corticostriatal drive was selectively enhanced in Tsc1 KO dSPNs (Figures 6E and 6F).

To understand how stronger corticostriatal input could affect dSPN activity, we measured cortically driven action potentials (oAPs) in simultaneously recorded pairs of dSPN WT and Tsc1 KO cells in the absence of synaptic blockers. To achieve robust cortical ChR2 expression sufficient to drive SPN firing, we bred *Tsc1*$^{fl/fl}$*;D1-tdTomato* mice to mice expressing ChR2-YFP under the *Thy1* promoter (*Thy1-ChR2-YFP*) (Arenkiel et al., 2007). Optical stimulation of corticostriatal terminals resulted in a significantly shorter latency to fire in Tsc1 KO dSPNs compared with simultaneously recorded controls (Figures 6G–6I). We also observed a trend toward decreased jitter in Tsc1 KO dSPNs (Figure 6J). These results demonstrate that loss of Tsc1 from dSPNs enhances corticostriatal transmission and alters their firing properties in response to cortical stimulation.

DISCUSSION

In this study, we determined how activation of mTORC1 signaling affects striatal physiology by deleting the mTORC1 negative regulator *Tsc1* from a subset of neurons in the dorsal striatum. With this approach, we gained an understanding of how TSC-mTORC1 signaling

affects SPN morphology and function in a cell autonomous manner, independent of major network or developmental alterations. We found that the primary effect of Tsc1 loss was an increase in dSPN excitability with minimal effects on iSPNs. Both intrinsic and corticostriatal synaptic excitability were enhanced by deletion of *Tsc1* from dSPNs without concurrent changes to synaptic inhibition or thalamostriatal excitation. The net effect of these changes was decreased latency of Tsc1 KO dSPNs to fire in response to cortical stimulation. These findings demonstrate that loss of Tsc1 and constitutive activation of mTORC1 signaling strongly affect the properties of direct pathway neurons such that cortical excitation is facilitated, with relatively little impact on neurons comprising the indirect pathway.

An interesting aspect of our study is the observed increase in dSPN, but not iSPN, intrinsic excitability due to postnatal loss of Tsc1. The increased excitability of Tsc1 KO dSPNs contrasts with the reduced excitability that has been observed in other cell types with Tsc1 loss, including hippocampal CA1 neurons, thalamic neurons, and Purkinje cells (Bateup et al., 2013; Normand et al., 2013; Tsai et al., 2012). Compared with these cell types, we observed a relatively modest increase in soma size in Tsc1 KO SPNs (a 14% increase in SPNs versus a 41% increase in CA1 neurons with Tsc1 loss; Bateup et al., 2011). We also found that dendritic arborization was reduced in Tsc1 KO dSPNs. This decreased dendritic complexity likely has a stronger impact on the cell's passive membrane properties than the small increase in soma size, leading to a net decrease in membrane capacitance and increase in resistance. These changes in passive membrane properties, together with the reduced Kir currents we observed, likely drive increased excitability in Tsc1 KO dSPNs. The fact that Tsc1 KO iSPNs showed a similar small increase in soma size as dSPNs but did not have major changes in dendritic morphology or Kir currents further indicates that these factors were responsible for the excitability changes in Tsc1 KO dSPNs. Notably, loss of Tsc1 has been shown to have cell-type-specific effects on the excitability of hypothalamic neurons, whereby *Pomc*-expressing Tsc1 KO neurons exhibit hypoexcitability but *Agrp*-expressing Tsc1 KO neurons show no change in excitability (Yang et al., 2012).

Cell-type-specific changes in intrinsic excitability and den-dritic morphology have been observed in SPNs in response to a variety of disease-related insults. For example, intrinsic excitability is increased and dendritic arborization is decreased in dSPNs but not iSPNs in L-DOPA-induced dyskinesia, in which mTOR signaling is hyperactive (Fieblinger et al., 2014; Santini et al., 2009; Santini et al., 2012). Huntington's disease mouse models are associated with low mTOR signaling and display altered potassium currents as well as iSPN-specific degeneration (Lee et al., 2015; Mitchell et al., 1999; Tong et al., 2014). The fact that phenotypes specific to either dSPNs or iSPNs are seen across mTOR-associated diseases is likely due to molecular differences between the two SPN subtypes. Although dSPNs and iSPNs are similar in many respects, they express distinct profiles of receptors and signaling molecules (Heiman et al., 2008), which will define their response to disease-related perturbations. Because the mTOR pathway integrates a variety of intra- and extracellular signals and shows extensive cross-talk with other signaling pathways, the outcomes of its activation are highly sensitive to the cellular context. Here we find no differences in the basal phosphorylation state of the mTORC1 pathway target S6 between dSPNs and iSPNs. In addition, Tsc1 loss elevated p-S6 levels to a similar extent in dSPNs and iSPNs. These

observations suggest that the core components of mTORC1 signaling are not different between dSPNs and iSPNs but that the consequences of mTORC1 activation on downstream pathways differs by cell type.

Changes in synaptic transmission are often, but not always (Tsai et al., 2012), observed in response to loss of Tsc1 (Tavazoie et al., 2005; Bateup et al., 2011, 2013; Weston et al., 2014). In particular, a previous study showed that deletion of *Tsc1* from hippocampal CA1 neurons causes a loss of inhibitory synaptic transmission resulting in increased excitatory/inhibitory synaptic ratio (Bateup et al., 2013). Changes in E/I balance are hypothesized to contribute to ASD pathophysiology (Rubenstein and Merzenich, 2003), and a recent study showed cell-type-specific alterations in excitatory/inhibitory (E/I) ratio in dSPNs resulting from mutations in the ASD-risk gene *Nlgn3* (Rothwell et al., 2014). Here we found that synaptic E/I balance was also selectively altered in dSPNs following *Tsc1* deletion; however, this was driven by an increase in excitatory synaptic drive without a change in inhibition. The downstream consequences of increased E/I ratio in dSPNs remain to be explored, but such a change is likely to increase the efficacy of the direct pathway to suppress basal ganglia output nuclei, thereby relieving their inhibition of downstream motor centers (Kravitz et al., 2010; Roseberry et al., 2016). Notably, corticostriatal synaptic transmission was selectively increased in Tsc1 KO dSPNs, while thalamostriatal transmission was unaltered. Similar increases in corticostriatal transmission have been observed in the *Shank3B*$^{-/-}$ mouse model of autism and in the *Sapap3*$^{-/-}$ mouse model of obsessive-compulsive disorder (Peixoto et al., 2016; Wan et al., 2014), suggesting that enhanced corticostriatal activity in the dorsal striatum may be involved in the pathophysiology of multiple psychiatric disorders.

We found that the enhanced corticostriatal transmission in Tsc1 KO dSPNs was mediated by an increase in presynaptic release probability. This is supported by our observation of decreased paired-pulse ratio with no changes in mEPSC amplitude or dendritic spine density, which would indicate alterations in postsynaptic strength or synapse number, respectively. Because Cre expression was limited to striatal neurons in our model and the cortical inputs were WT for *Tsc1*, this suggests a change in retrograde signaling from SPN dendrites to cortical presynaptic terminals. Corticostriatal synapses are known to undergo endocannabinoid-dependent long-term depression (eCB-LTD), which is mediated by changes in presynaptic release probability (Surmeier et al., 2009). It is possible that deregulated mTORC1 signaling interferes with the production or release of retrograde signaling molecules from dSPNs, a direction that could be explored in future studies. Such a mechanism may also explain the input specificity of the phenotype, as thalamostriatal synapses do not undergo substantial eCB-LTD (Wu et al., 2015).

The relative timing of activation of the direct and indirect pathways is important for habit formation (O'Hare et al., 2016). For example, shorter latency of dSPNs to fire relative to iSPNs in response to cortical stimulation is correlated with preference to use more habitual strategies when learning an operant task (O'Hare et al., 2016). Interestingly, we found that *Tsc1* deletion caused dSPNs to fire with reduced latency in response to cortical stimulation. Furthermore, there was a trend toward decreased action potential jitter in Tsc1 KO dSPNs across multiple stimulation trials, which could have implications for spike timing-dependent

plasticity (Shen et al., 2008). These results suggest that loss of Tsc1 and upregulation of mTORC1 in SPNs enhances cortical activation of the direct pathway. Future studies will determine if these cellular changes result in altered striatal-associated behaviors, with the goal of understanding how striatal dysfunction contributes to psychiatric disorders such as ASD.

EXPERIMENTAL PROCEDURES

Mice

Animal experiments were performed in accordance with protocols approved by the University of California, Berkeley, Animal Care and Use Committee. Male and female mice were used for all experiments. Please see Supplemental Experimental Procedures for a list of mouse lines used and a detailed description of the methods.

Stereotaxic Surgery

800nl of an AAV5 chicken b-actin promoter-driven Cre-mCherry or Cre-GFP virus (Penn Vector Core) was unilaterally injected into the dorsolateral striatum of postnatal day (P) 14–16 *Tsc1*$^{fl/fl}$*;D2-GFP* or *Tsc1*$^{fl/fl}$*;D1-tdTomato* mice, respectively. Cre virus was diluted 20–30 times in sterile saline to achieve sparse transduction. Mice were used for experiments 11–15 days after Cre virus injection.

For the oIPSC experiments, Flp-dependent, *Ef1a* promoter-driven AAV5-fDIO-ChR2-EYFP virus (Fenno et al., 2014) was injected unilaterally into the dorsolateral striatum of P15–P17 *Tsc1;D1-tdTomato;Pvalb-2A-FlpO-D* mice, followed by injection of AAV5-Cre-GFP at P34–P37. For oAP experiments, *Tsc1*$^{fl/fl}$*;D1-tdTomato;Thy1-ChR2-YFP* mice were injected with AAV5-Cre-GFP into the dorsolateral striatum at P20–P27. For oEPSP experiments, CAG promoter-driven AAV5-ChR2-mCherry was injected into either the cortex or thalamus of neonatal mice. At P14–P16, AAV5-Cre-GFP virus was injected into the dorsolateral striatum as described above. Injection coordinates are listed in the Supplemental Experimental Procedures.

Immunohistochemistry

P25–P31 mice were perfused transcardially. Brains were post-fixed in 4% paraformaldehyde overnight and sectioned at 30 μm. Sections were blocked for 1 hr at room temperature (RT) in BlockAid (Thermo Fisher Scientific) and incubated overnight at 4°C with antibodies against phosphorylated (Ser240/244) S6 ribosomal protein (1:800; catalog no. 5364S, Cell Signaling Technology), GFP (1:5,000; catalog no. ab13970, Abcam) and NeuN (1:800; catalog no. MAB377, Millipore). Sections were washed and incubated for 1 hr at RT with Alexa Fluor 633-, 488-, and 405-conjugated secondary antibodies (1:500; catalog nos. A-21070, A11039, and A-31553, Invitrogen). Sections were mounted onto slides using ProLong Gold antifade reagent (Invitrogen).

Imaging and Analysis

Z stack images were taken on a confocal microscope (Olympus Fluoview FV1000) with a 203 objective using the same exposure and acquisition settings for each section. To quantify

p-S6 levels and soma volume, regions of interest (ROIs) were automatically generated in Imaris software based on the NeuN or D2-GFP signal. The mean p-S6 fluorescence intensity per ROI and average soma volume were calculated using Imaris.

Dendrite Morphology Reconstruction

For anatomical reconstruction, 4 mg/mL neurobiotin was included in the internal solution during whole-cell recordings. Slices were recovered and fixed in 4% paraformaldehyde for 24–48 hr. After washes in PBS, slices were reacted with 1:750 streptavidin-Alexa Fluor 633 (Invitrogen) for 1 h. Sections were then washed and coverslipped using ProLong Gold antifade reagent. Dendrite arborization was quantified using 3D Sholl analysis in Imaris software. For dendritic spine analysis, proximal (50 μm from soma) and distal (100 μm from soma) dendrites were imaged on a Zeiss LSM 880 NLO AxioExaminer with Airyscan. Dendrites and spines were reconstructed in three dimensions and analyzed in Imaris.

Electrophysiology

Mice were perfused transcardially with ice-cold ACSF (pH 7.4) containing 127 mM NaCl, 25 mM $NaHCO_3$, 1.25 mM NaH_2PO_4, 2.5 mM KCl, 1 mM $MgCl_2$, 2 mM $CaCl_2$, and 25 mM glucose. Brains were rapidly removed, and coronal slices (275 μm) were cut on a VT1000S vibrotome (Leica) in oxygenated ice-cold choline-based external solution (pH 7.8) containing 110 mM choline chloride, 25 mM $NaHCO_3$, 1.25 mM $NaHPO_4$, 2.5 mM KCl, 7 mM $MgCl_2$, 0.5 mM $CaCl_2$, 25 mM glucose, 11.6 mM sodium ascorbate, and 3.1 mM sodium pyruvate. Slices were recovered in ACSF at 34 C for 15 min and then kept at RT. Recordings were made with a MultiClamp 700B amplifier (Molecular Devices) at RT using 3–5 MU glass patch electrodes. Current-clamp recordings were made using a potassium-based internal solution (pH 7.4) containing 135 mM $KMeSO_4$, 5 mM KCl, 5 mM HEPES, 4 mM Mg-ATP, 0.3 mM Na-GTP, 10 mM phosphocreatine, and 1 mM EGTA. Voltage-clamp recordings were made using a cesium-based internal solution (pH 7.4) containing 120 mM $CsMeSO_4$, 15 mM CsCl, 10 mM TEA-Cl, 8 mM NaCl, 10 mM HEPES, 0.2–5 mM EGTA, 5 mM QX-314, 4 mM Mg-ATP, and 0.3 mM Na-GTP. For eIPSC experiments, recordings were made using a high chloride cesium-based internal solution (pH 7.2) to maximize IPSC amplitude, containing 125 mM CsCl, 10 mM TEA-Cl, 10 mM HEPES, 4 mM Mg-ATP, 0.3 mM Na-GTP, 8 mM Na_2CrePO_4, 0.1 mM EGTA, and 3.3 mM QX-314. For experiments measuring synaptic currents, cells were held at −80 mV, and recordings were acquired with the amplifier's Bessel filter set at 3 kHz.

Statistical Analyses

Two-tailed paired or unpaired t tests were used for comparisons between two groups. A one-way ANOVA with Sidak's post hoc test was used to compare the means of three or more groups. A two-way ANOVA with Sidak's post hoc test was used to compare mean differences between groups for experiments with two independent variables. p values were corrected for multiple comparisons. For data that did not pass the D'Agostino and Pearson normality test, the Kruskal-Wallis with Dunn's post hoc test was used. Cumulative distributions were analyzed using the K-S test. Values for all statistical comparisons are provided in Tables S1–S4.

Supplementary Material

Refer to Web version on PubMed Central for supplementary material.

Acknowledgments

We thank the members of the Bateup lab for their feedback on this work. This project was supported by Simons Foundation Autism Research Initiative (SFARI) Pilot Award 307866 and National Institute of Mental Health (NIMH) grant R56MH111821. H.S.B. is supported by a fellowship from the Alfred P. Sloan Foundation (FR-2015-65790). K.N.B. is supported by the National Science Foundation Graduate Research Fellowship under grant DGE 1106400.

References

Arenkiel BR, Peca J, Davison IG, Feliciano C, Deisseroth K, Augustine GJ, Ehlers MD, Feng G. In vivo light-induced activation of neural circuitry in transgenic mice expressing channelrhodopsin-2. Neuron. 2007; 54:205–218. [PubMed: 17442243]

Bateup HS, Santini E, Shen W, Birnbaum S, Valjent E, Surmeier DJ, Fisone G, Nestler EJ, Greengard P. Distinct subclasses of medium spiny neurons differentially regulate striatal motor behaviors. Proc Natl Acad Sci U S A. 2010; 107:14845–14850. [PubMed: 20682746]

Bateup HS, Takasaki KT, Saulnier JL, Denefrio CL, Sabatini BL. Loss of Tsc1 in vivo impairs hippocampal mGluR-LTD and increases excitatory synaptic function. J Neurosci. 2011; 31:8862–8869. [PubMed: 21677170]

Bateup HS, Johnson CA, Denefrio CL, Saulnier JL, Kornacker K, Sabatini BL. Excitatory/inhibitory synaptic imbalance leads to hippocampal hyperexcitability in mouse models of tuberous sclerosis. Neuron. 2013; 78:510–522. [PubMed: 23664616]

Cazorla M, Shegda M, Ramesh B, Harrison NL, Kellendonk C. Striatal D2 receptors regulate dendritic morphology of medium spiny neurons via Kir2 channels. J Neurosci. 2012; 32:2398–2409. [PubMed: 22396414]

Costa-Mattioli M, Monteggia LM. mTOR complexes in neurodevelopmental and neuropsychiatric disorders. Nat Neurosci. 2013; 16:1537–1543. [PubMed: 24165680]

Crino PB. Evolving neurobiology of tuberous sclerosis complex. Acta Neuropathol. 2013; 125:317–332. [PubMed: 23386324]

Crino PB, Nathanson KL, Henske EP. The tuberous sclerosis complex. N Engl J Med. 2006; 355:1345–1356. [PubMed: 17005952]

Curatolo P, Napolioni V, Moavero R. Autism spectrum disorders in tuberous sclerosis: pathogenetic pathways and implications for treatment. J Child Neurol. 2010; 25:873–880. [PubMed: 20207609]

Curatolo P, Moavero R, de Vries PJ. Neurological and neuropsychiatric aspects of tuberous sclerosis complex. Lancet Neurol. 2015; 14:733–745. [PubMed: 26067126]

Davis PE, Peters JM, Krueger DA, Sahin M. Tuberous sclerosis: a new frontier in targeted treatment of autism. Neurotherapeutics. 2015; 12:572–583. [PubMed: 25986747]

Ehninger D, Han S, Shilyansky C, Zhou Y, Li W, Kwiatkowski DJ, Ramesh V, Silva AJ. Reversal of learning deficits in a Tsc2+/− mouse model of tuberous sclerosis. Nat Med. 2008; 14:843–848. [PubMed: 18568033]

Fenno LE, Mattis J, Ramakrishnan C, Hyun M, Lee SY, He M, Tucciar-one J, Selimbeyoglu A, Berndt A, Grosenick L, et al. Targeting cells with single vectors using multiple-feature Boolean logic. Nat Methods. 2014; 11:763–772. [PubMed: 24908100]

Fieblinger T, Graves SM, Sebel LE, Alcacer C, Plotkin JL, Gertler TS, Chan CS, Heiman M, Greengard P, Cenci MA, Surmeier DJ. Cell type-specific plasticity of striatal projection neurons in parkinsonism and L-DOPA-induced dyskinesia. Nat Commun. 2014; 5:5316. [PubMed: 25360704]

Fuccillo MV. Striatal circuits as a common node for autism pathophysiology. Front Neurosci. 2016; 10:27. [PubMed: 26903795]

Gerfen CR, Surmeier DJ. Modulation of striatal projection systems by dopamine. Annu Rev Neurosci. 2011; 34:441–466. [PubMed: 21469956]

Gertler TS, Chan CS, Surmeier DJ. Dichotomous anatomical properties of adult striatal medium spiny neurons. J Neurosci. 2008; 28:10814–10824. [PubMed: 18945889]

Gittis AH, Kreitzer AC. Striatal microcircuitry and movement disorders. Trends Neurosci. 2012; 35:557–564. [PubMed: 22858522]

Graybiel AM. The basal ganglia: learning new tricks and loving it. Curr Opin Neurobiol. 2005; 15:638–644. [PubMed: 16271465]

Graybiel AM, Grafton ST. The striatum: where skills and habits meet. Cold Spring Harb Perspect Biol. 2015; 7:a021691. [PubMed: 26238359]

Gunaydin LA, Kreitzer AC. Cortico-basal ganglia circuit function in psychiatric disease. Annu Rev Physiol. 2016; 78:327–350. [PubMed: 26667072]

Heiman M, Schaefer A, Gong S, Peterson JD, Day M, Ramsey KE, Suárez-Fariñas M, Schwarz C, Stephan DA, Surmeier DJ, et al. A translational profiling approach for the molecular characterization of CNS cell types. Cell. 2008; 135:738–748. [PubMed: 19013281]

Hoeffer CA, Klann E. mTOR signaling: at the crossroads of plasticity, memory and disease. Trends Neurosci. 2010; 33:67–75. [PubMed: 19963289]

Huber KM, Klann E, Costa-Mattioli M, Zukin RS. Dysregulation of mammalian target of rapamycin signaling in mouse models of autism. J Neurosci. 2015; 35:13836–13842. [PubMed: 26468183]

Klaus A, Martins GJ, Paixao VB, Zhou P, Paninski L, Costa RM. The spatiotemporal organization of the striatum encodes action space. Neuron. 2017; 95:1171–1180.e7. [PubMed: 28858619]

Koós T, Tepper JM. Inhibitory control of neostriatal projection neurons by GABAergic interneurons. Nat Neurosci. 1999; 2:467–472. [PubMed: 10321252]

Kravitz AV, Freeze BS, Parker PR, Kay K, Thwin MT, Deisseroth K, Kreitzer AC. Regulation of parkinsonian motor behaviours by optogenetic control of basal ganglia circuitry. Nature. 2010; 466:622–626. [PubMed: 20613723]

Kreitzer AC. Physiology and pharmacology of striatal neurons. Annu Rev Neurosci. 2009; 32:127–147. [PubMed: 19400717]

Kreitzer AC, Malenka RC. Striatal plasticity and basal ganglia circuit function. Neuron. 2008; 60:543–554. [PubMed: 19038213]

Lee JH, Tecedor L, Chen YH, Monteys AM, Sowada MJ, Thompson LM, Davidson BL. Reinstating aberrant mTORC1 activity in Huntington's disease mice improves disease phenotypes. Neuron. 2015; 85:303–315. [PubMed: 25556834]

Lipton JO, Sahin M. The neurology of mTOR. Neuron. 2014; 84:275–291. [PubMed: 25374355]

Madisen L, Zwingman TA, Sunkin SM, Oh SW, Zariwala HA, Gu H, Ng LL, Palmiter RD, Hawrylycz MJ, Jones AR, et al. A robust and high-throughput Cre reporting and characterization system for the whole mouse brain. Nat Neurosci. 2010; 13:133–140. [PubMed: 20023653]

Meikle L, Talos DM, Onda H, Pollizzi K, Rotenberg A, Sahin M, Jensen FE, Kwiatkowski DJ. A mouse model of tuberous sclerosis: neuronal loss of Tsc1 causes dysplastic and ectopic neurons, reduced myelination, seizure activity, and limited survival. J Neurosci. 2007; 27:5546–5558. [PubMed: 17522300]

Mink JW. The basal ganglia and involuntary movements: impaired inhibition of competing motor patterns. Arch Neurol. 2003; 60:1365–1368. [PubMed: 14568805]

Mitchell IJ, Cooper AJ, Griffiths MR. The selective vulnerability of striatopallidal neurons. Prog Neurobiol. 1999; 59:691–719. [PubMed: 10845758]

Normand EA, Crandall SR, Thorn CA, Murphy EM, Voelcker B, Browning C, Machan JT, Moore CI, Connors BW, Zervas M. Temporal and mosaic Tsc1 deletion in the developing thalamus disrupts thalamocortical circuitry, neural function, and behavior. Neuron. 2013; 78:895–909. [PubMed: 23664552]

O'Hare JK, Ade KK, Sukharnikova T, Van Hooser SD, Palmeri ML, Yin HH, Calakos N. Pathway-specific striatal substrates for habitual behavior. Neuron. 2016; 89:472–479. [PubMed: 26804995]

Peixoto RT, Wang W, Croney DM, Kozorovitskiy Y, Sabatini BL. Early hyperactivity and precocious maturation of corticostriatal circuits in Shank3B(−/−) mice. Nat Neurosci. 2016; 19:716–724. [PubMed: 26928064]

Roseberry TK, Lee AM, Lalive AL, Wilbrecht L, Bonci A, Kreitzer AC. Cell-type-specific control of brainstem locomotor circuits by basal ganglia. Cell. 2016; 164:526–537. [PubMed: 26824660]

Rothwell PE, Fuccillo MV, Maxeiner S, Hayton SJ, Gokce O, Lim BK, Fowler SC, Malenka RC, Südhof TC. Autism-associated neuroligin-3 mutations commonly impair striatal circuits to boost repetitive behaviors. Cell. 2014; 158:198–212. [PubMed: 24995986]

Rubenstein JL, Merzenich MM. Model of autism: increased ratio of excitation/inhibition in key neural systems. Genes Brain Behav. 2003; 2:255–267. [PubMed: 14606691]

Santini E, Heiman M, Greengard P, Valjent E, Fisone G. Inhibition of mTOR signaling in Parkinson's disease prevents L-DOPA–induced dyskinesia. Neuroscience. 2009; 2:1–11.

Santini E, Feyder M, Gangarossa G, Bateup HS, Greengard P, Fisone G. Dopamine- and cAMP-regulated phosphoprotein of 32-kDa (DARPP-32)-dependent activation of extracellular signal-regulated kinase (ERK) and mammalian target of rapamycin complex 1 (mTORC1) signaling in experimental parkinsonism. J Biol Chem. 2012; 287:27806–27812. [PubMed: 22753408]

Saxton RA, Sabatini DM. mTOR signaling in growth, metabolism, and disease. Cell. 2017; 168:960–976. [PubMed: 28283069]

Shen W, Tian X, Day M, Ulrich S, Tkatch T, Nathanson NM, Surmeier DJ. Cholinergic modulation of Kir2 channels selectively elevates dendritic excitability in striatopallidal neurons. Nat Neurosci. 2007; 10:1458–1466. [PubMed: 17906621]

Shen W, Flajolet M, Greengard P, Surmeier DJ. Dichotomous dopaminergic control of striatal synaptic plasticity. Science. 2008; 321:848–851. [PubMed: 18687967]

Smith Y, Bevan MD, Shink E, Bolam JP. Microcircuitry of the direct and indirect pathways of the basal ganglia. Neuroscience. 1998; 86:353–387. [PubMed: 9881853]

Smith Y, Surmeier DJ, Redgrave P, Kimura M. Thalamic contributions to Basal Ganglia-related behavioral switching and reinforcement. J Neurosci. 2011; 31:16102–16106. [PubMed: 22072662]

Subramanian M, Timmerman CK, Schwartz JL, Pham DL, Meffert MK. Characterizing autism spectrum disorders by key biochemical pathways. Front Neurosci. 2015; 9:313. [PubMed: 26483618]

Surmeier DJ, Plotkin J, Shen W. Dopamine and synaptic plasticity in dorsal striatal circuits controlling action selection. Curr Opin Neurobiol. 2009; 19:621–628. [PubMed: 19896832]

Tavazoie SF, Alvarez VA, Ridenour DA, Kwiatkowski DJ, Sabatini BL. Regulation of neuronal morphology and function by the tumor suppressors Tsc1 and Tsc2. Nat Neurosci. 2005; 8:1727–1734. [PubMed: 16286931]

Tepper JM, Tecuapetla F, Koós T, Ibáñez-Sandoval O. Heterogeneity and diversity of striatal GABAergic interneurons. Front Neuroanat. 2010; 4:150. [PubMed: 21228905]

Tong X, Ao Y, Faas GC, Nwaobi SE, Xu J, Haustein MD, Anderson MA, Mody I, Olsen ML, Sofroniew MV, Khakh BS. Astrocyte Kir4.1 ion channel deficits contribute to neuronal dysfunction in Huntington's disease model mice. Nat Neurosci. 2014; 17:694–703. [PubMed: 24686787]

Tsai PT, Hull C, Chu Y, Greene-Colozzi E, Sadowski AR, Leech JM, Steinberg J, Crawley JN, Regehr WG, Sahin M. Autistic-like behaviour and cerebellar dysfunction in Purkinje cell Tsc1 mutant mice. Nature. 2012; 488:647–651. [PubMed: 22763451]

Wan Y, Ade KK, Caffall Z, Ilcim Ozlu M, Eroglu C, Feng G, Calakos N. Circuit-selective striatal synaptic dysfunction in the Sapap3 knockout mouse model of obsessive-compulsive disorder. Biol Psychiatry. 2014; 75:623–630. [PubMed: 23414593]

Weston MC, Chen H, Swann JW. Loss of mTOR repressors Tsc1 or Pten has divergent effects on excitatory and inhibitory synaptic transmission in single hippocampal neuron cultures. Front Mol Neurosci. 2014; 7:1. [PubMed: 24574959]

Wilson CJ, Kawaguchi Y. The origins of two-state spontaneous membrane potential fluctuations of neostriatal spiny neurons. J Neurosci. 1996; 16:2397–2410. [PubMed: 8601819]

Wu YW, Kim JI, Tawfik VL, Lalchandani RR, Scherrer G, Ding JB. Input- and cell-type-specific endocannabinoid-dependent LTD in the striatum. Cell Rep. 2015; 10:75–87. [PubMed: 25543142]

Yang SB, Tien AC, Boddupalli G, Xu AW, Jan YN, Jan LY. Rapamycin ameliorates age-dependent obesity associated with increased mTOR signaling in hypothalamic POMC neurons. Neuron. 2012; 75:425–436. [PubMed: 22884327]

Highlights

- Postnatal loss of Tsc1 causes hyperexcitability of dSPNs but not iSPNs
- Tsc1 KO dSPNs have altered somatic and dendritic morphology
- Tsc1 KO dSPNs have increased excitatory synaptic drive with no change in inhibition
- Corticostriatal transmission is selectively enhanced onto Tsc1 KO dSPNs

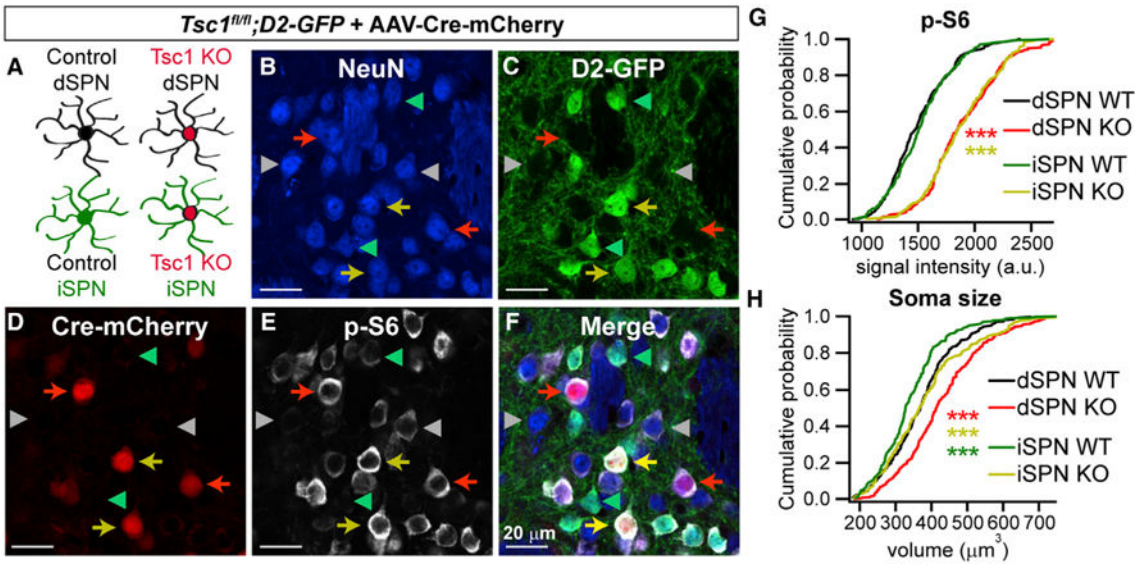

Figure 1. Mosaic Loss of *Tsc1* from Striatal Neurons Induces mTORC1 Activation and Somatic Hypertrophy

(A) Schematic showing the four cell types present in each striatal slice of a *Tsc1*$^{fl/fl}$;*D2-GFP* mouse injected with AAV5-Cre-mCherry. iSPNs are identified by GFP fluorescence, and Tsc1 KO neurons are identified by nuclear mCherry expression.

(B–F) Confocal images of a striatal section showing NeuN immunostaining (B), D2-GFP fluorescence (C), Cre-mCherry fluorescence (D), phosphorylated S6 immunostaining (p-S6, Ser240/244) (E), and a merged image (F). Red arrows show Tsc1 KO dSPNs, yellow arrows show Tsc1 KO iSPNs, grey arrowheads indicate WT dSPNs and green arrowheads indicate WT iSPNs.

(G and H) Cumulative distributions of p-S6 levels (G) and soma volume (H) for neurons of each genotype. n = 300 neurons per genotype from 3 mice, 100 neurons per mouse. ***p < 0.0001, K-S test; red stars indicate significance for dSPN KO versus dSPN WT, yellow stars denote significance for iSPN KO versus iSPN WT, and green stars indicate significance for dSPN WT versus iSPN WT.

See also Figure S1.

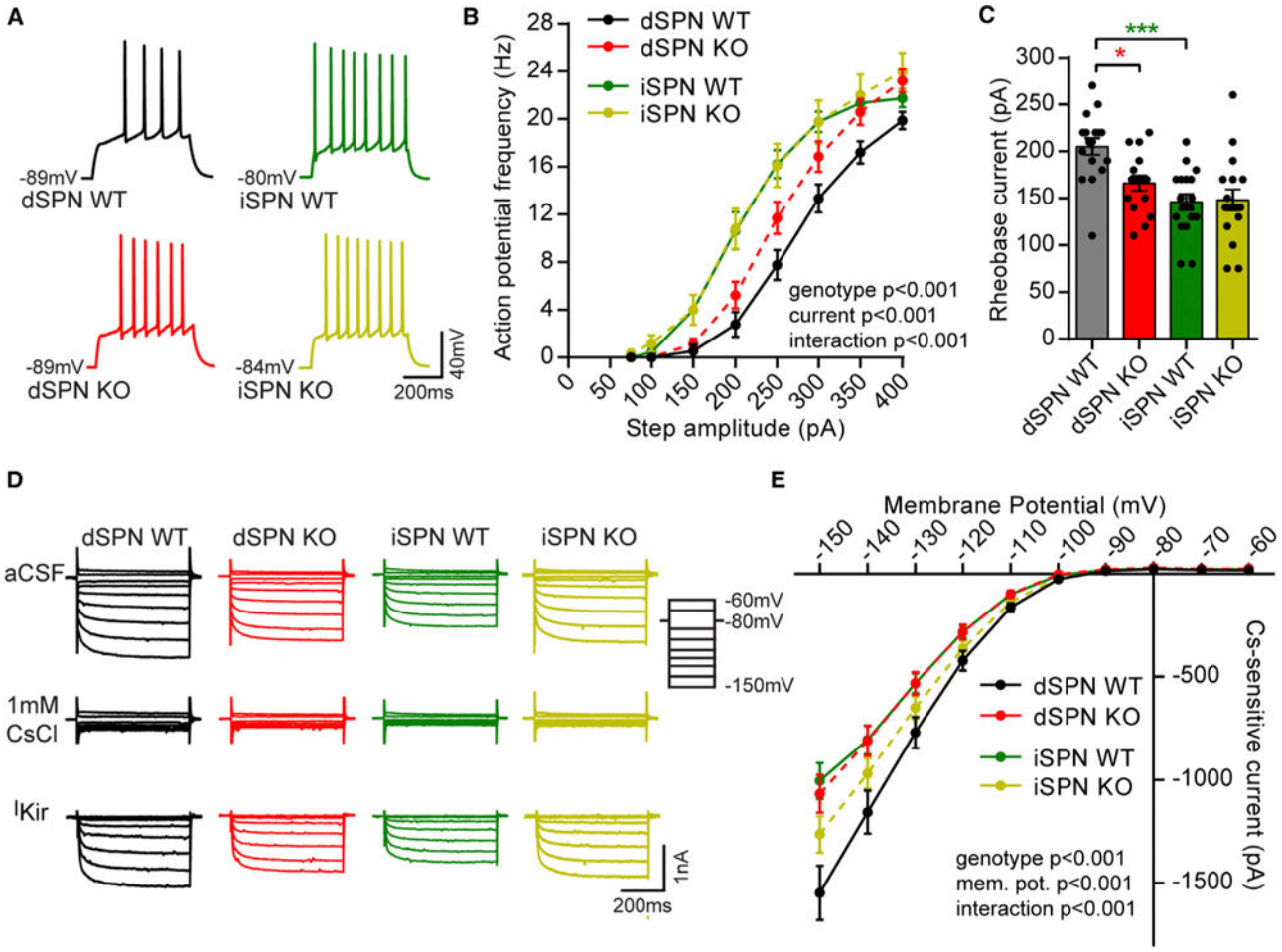

Figure 2. Postnatal Loss of *Tsc1* Increases the Intrinsic Excitability of dSPNs

(A) Example traces showing action potentials evoked by a 250 pA current step for each cell type. The resting membrane potential is indicated to the left of each trace.

(B) Frequency-current relationship for control (WT) and Tsc1 KO dSPNs and iSPNs, displayed as mean ± SEM. Two-way ANOVA p values are shown. p values for Sidak's post hoc tests are in Table S1. dSPN WT n = 18 neurons from 15 mice, dSPN KO n = 21 neurons from 14 mice, iSPN WT n = 18 neurons from 16 mice, and iSPN KO n = 17 neurons from 13 mice.

(C) Bar graph shows the mean ± SEM rheobase for each condition. Dots indicate the values for individual neurons. *p < 0.05 and ***p < 0.001, one-way ANOVA with Sidak's post hoc test (see Table S2 for all p values); dSPN WT n = 17 neurons from 15 mice, dSPN KO n = 16 neurons from 13 mice, iSPN WT n = 18 neurons from 16 mice, and iSPN KO n = 17 neurons from 13 mice.

(D) Example traces of inward-rectifying potassium channel currents in dSPNs and iSPNs. Kir channel currents were obtained by applying negative voltage steps to the membrane (−150 to −60 mV in 10 mV increments) in the presence and absence of 1 mM CsCl. The cesium-sensitive component (I_{Kir}) was revealed using digital subtraction.

(E) Quantification of I_{Kir} at different membrane potentials across genotypes.

Data are represented as mean ± SEM. Two-way ANOVA p values are shown. p values for the Sidak's post hoc tests are in Table S2. dSPN WT n = 10 neurons from 10 mice, dSPN KO n = 10 neurons from 8 mice, iSPN WT n = 10 neurons from 10 mice, and iSPN KO n = 9 neurons from 9 mice.

See also Figure S1.

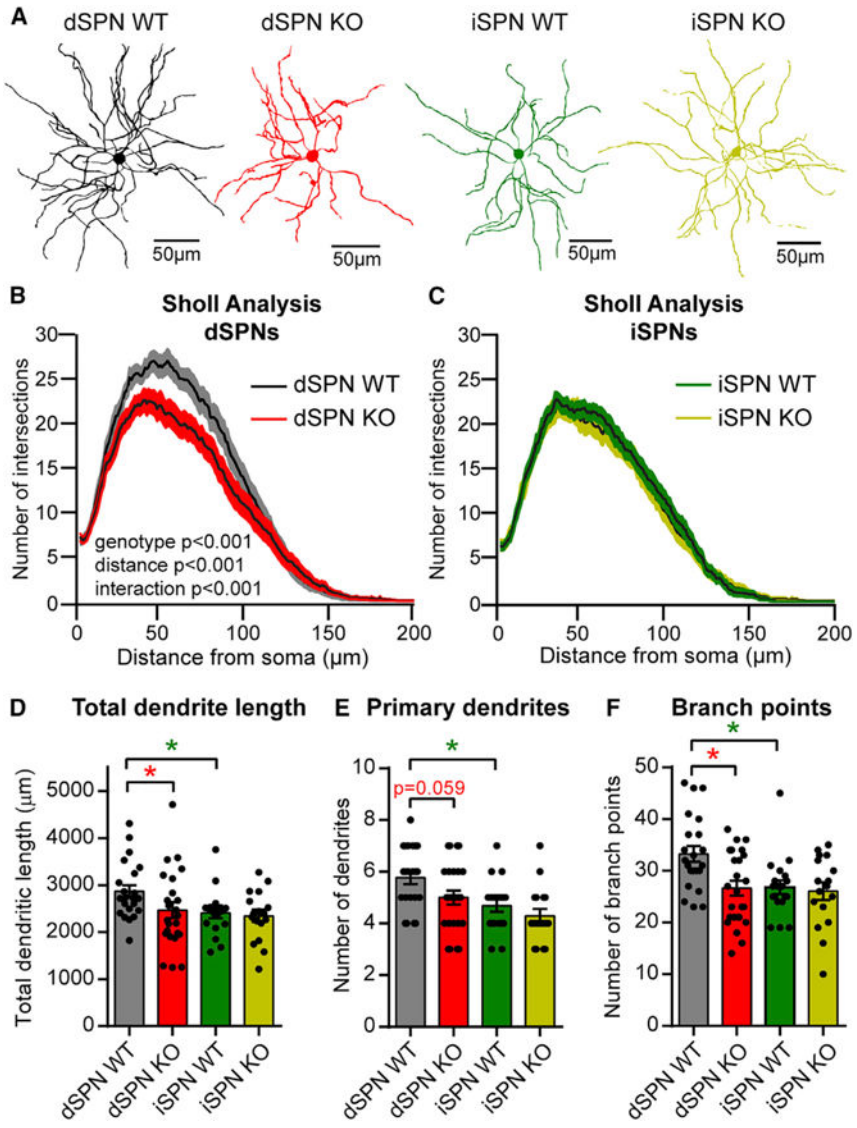

Figure 3. Tsc1 KO dSPNs Have Reduced Dendritic Arborization

(A) Example three-dimensional (3D) reconstructions of neurobiotin-filled SPNs of each condition. (B and C) Three-dimensional Sholl analysis of dSPN

(B) and iSPN (C) dendritic arbors. Circles of increasing radii were drawn at 1 μm intervals from the center of the soma and the number of dendrite crossings was quantified for each condition. Black lines indicate the mean and shaded regions show the SEM. Two-way ANOVA p values are shown for (B) and (C) combined (see also Table S1).

(D–F) Mean ± SEM of the total dendrite length (D), number of primary dendrites (E), and number of dendrite branch points (F) per neuron quantified by 3D Sholl analysis for each condition.

Dots indicate the values for individual neurons. *p < 0.05, Kruskal-Wallis with Dunn's post hoc test (total dendrite length and number of branch points; see Table S3 for p values) and one-way ANOVA with Sidak's post hoc test (number of primary dendrites; see Table S2 for p values). For all graphs, dSPN WT n = 22 neurons from 21 mice, dSPN KO n = 24 neurons

from 19 mice, iSPN WT n = 19 neurons from 19 mice, and iSPN KO n = 17 neurons from 16 mice.

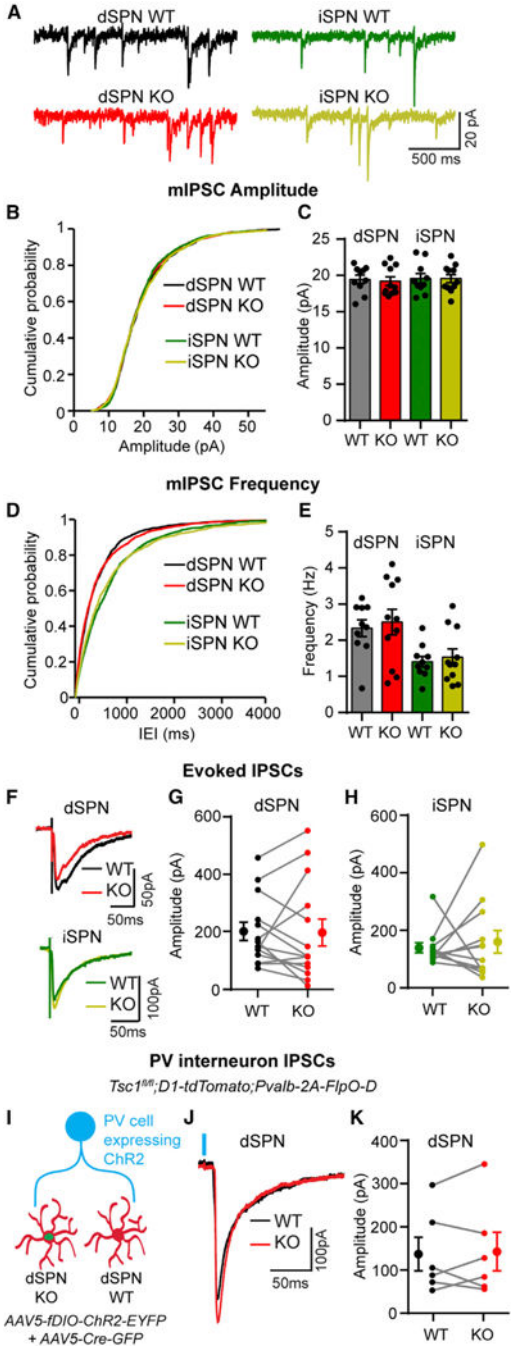

Figure 4. Inhibitory Synaptic Transmission onto SPNs Is Not Affected by Loss of Tsc1

(A) Example traces of miniature inhibitory postsynaptic currents (mIPSCs) recorded from each cell type.

(B) Cumulative distribution of mIPSC amplitudes from neurons of each genotype.

(C) Mean ± SEM mIPSC amplitude per neuron for each genotype.

(D) Cumulative distribution of mIPSC inter-event intervals (IEIs) from neurons of each genotype.

(E) Mean ± SEM mIPSC frequency per neuron. For (B)–(E), n = 200 mIPSCs per neuron, dSPN WT n = 10 neurons from 7 mice, dSPN KO n = 11 neurons from 8 mice, iSPN WT n = 10 neurons from 9 mice, and iSPN KO n = 11 neurons from 9 mice.

(F) Examples of simultaneously recorded IPSCs from pairs of Tsc1 WT and KO dSPNs and iSPNs, evoked by intra-striatal electrical stimulation.

(G and H) Graphs displaying the IPSC amplitude recorded from pairs of Tsc1 WT and KO dSPNs (G; n = 14 pairs from 10 mice) and iSPNs (H; n = 12 pairs from 10 mice).

(I) An AAV5-expressing Flp-dependent ChR2 was injected into the striatum of *Tsc1*$^{fl/fl}$*;D1-tdTomato;Pvalb-2A-FlpO-D* mice, followed by injection of AAV5-Cre-GFP. Paired recordings were made between Tsc1 WT and KO dSPNs, and PV-neuron inputs were activated by blue light stimulation.

(J) Examples of simultaneously recorded PV-IPSCs from a pair of Tsc1 WT and KO dSPNs, evoked by optogenetic stimulation. Blue line indicates light onset.

(K) Graph displaying the PV-IPSC amplitude recorded in pairs of Tsc1 WT and KO dSPNs, n = 6 pairs from 6 mice.

For all panels, dots indicate the values of individual neurons.

For (G), (H), and (K), the filled circles with error bars indicate the group mean ± SEM. See Tables S2 and S4 for p values for statistical comparisons.

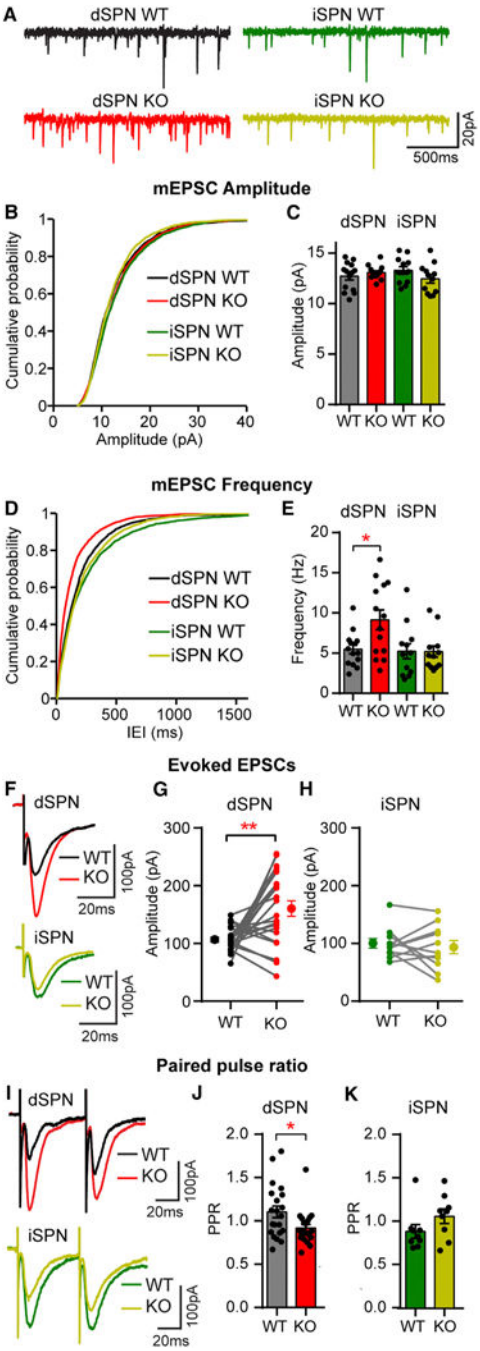

Figure 5. Excitatory Synaptic Transmission Is Increased in Tsc1 KO dSPNs

(A) Example traces of miniature excitatory postsynaptic currents (mEPSCs) recorded from each cell type.

(B) Cumulative distribution of mEPSC amplitudes from neurons of each genotype.

(C) Mean ± SEM mEPSC amplitude per neuron for each genotype.

(D) Cumulative distribution of mEPSC inter-event intervals (IEIs) from neurons of each genotype.

(E) Mean ± SEM mEPSC frequency per neuron. *p < 0.05, one-way ANOVA with Sidak's post hoc test. For (B)–(E), n = 200 mEPSCs per neuron, dSPN WT n = 14 neurons from 10 mice, dSPN KO n = 14 neurons from 10 mice, iSPN WT n = 12 neurons from 8 mice, and iSPN KO n = 12 neurons from 8 mice.

(F) Examples of simultaneously recorded EPSCs from Tsc1 WT and KO pairs of dSPN and iSPNs evoked by intra-striatal electrical stimulation.

(G and H) Graphs displaying the EPSC amplitude recorded from pairs of Tsc1 WT and KO dSPNs (G; n = 22 pairs from 19 mice) and iSPNs (H; n = 11 pairs from 6 mice). **p < 0.01, paired t test. Filled circles with error bars indicate the group mean ± SEM.

(I) Example recordings of electrically evoked EPSCs from two stimuli delivered 50 ms apart.

(J and K) Mean ± SEM paired pulse ratio (PPR; defined as the amplitude of the second EPSC peak divided by the first) in Tsc1 WT and KO dSPNs (J; n = 21 cells from 19 mice) and iSPNs (K; n = 9 cells from 6 mice). *p < 0.05, unpaired t test.

For all panels, dots indicate the values of individual neurons. See Tables S2 and S4 for p values for statistical comparisons. See also Figure S2.

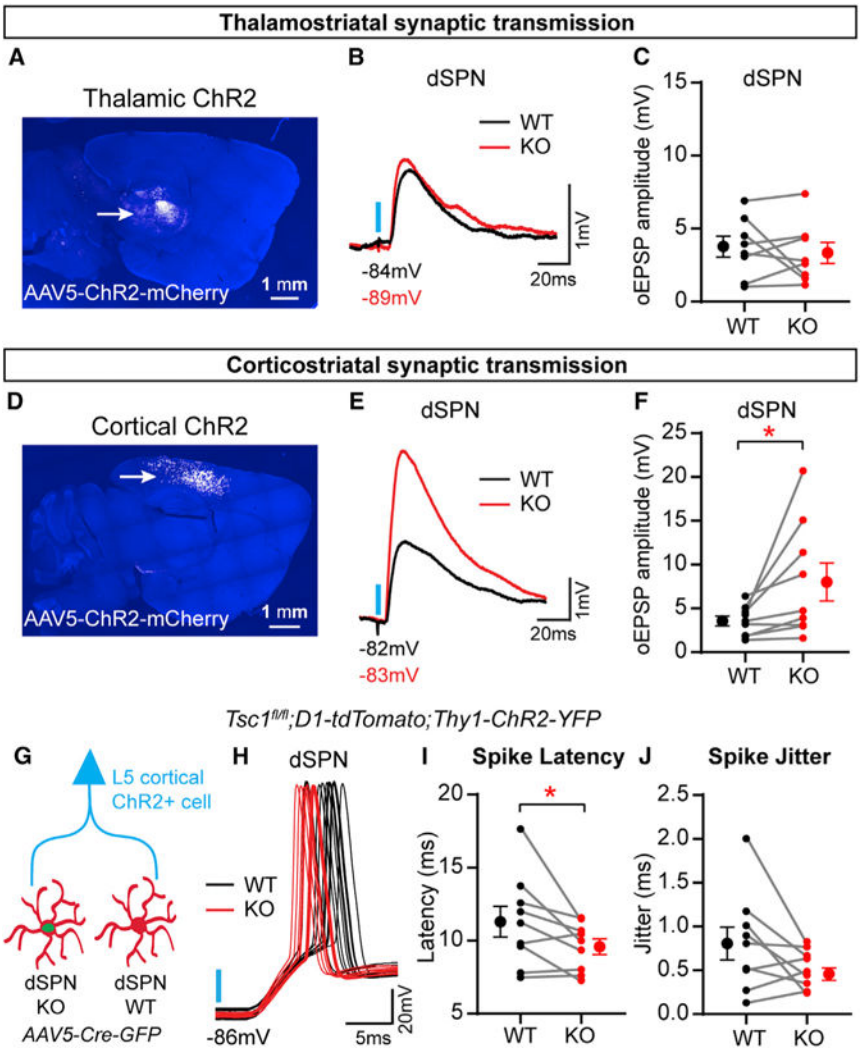

Figure 6. Corticostriatal Synaptic Transmission Is Selectively Enhanced in Tsc1 KO dSPNs

(A) AAV5-ChR2-mCherry was injected into the thalamus of neonate *Tsc1$^{fl/fl}$;D1-tdTomato* mice, followed by injection of AAV5-Cre-GFP into the dorsal striatum at P14–P16. Confocal image of a sagittal section showing ChR2-mCherry expression in the thalamus (arrow). DAPI staining is in blue.

(B) Examples of simultaneously recorded excitatory postsynaptic potentials (EPSPs) from a pair of Tsc1 WT and KO dSPNs, evoked by blue light stimulation of thalamostriatal terminals (blue line).

(C) Graph displaying thalamostriatal optogenetically evoked EPSP (oEPSP) amplitude recorded in pairs of Tsc1 WT and KO dSPNs, n = 8 pairs of neurons from five mice.

(D) AAV5-ChR2-mCherry was injected into the cortex of neonate *Tsc1$^{fl/fl}$;D1-tdTomato* mice, followed by injection of AAV5-Cre-GFP into the dorsal striatum at P14–P16. Confocal image of a sagittal section showing ChR2-mCherry expression in the cortex (arrow). DAPI staining is in blue.

(E) Examples of simultaneously recorded EPSPs from a pair of Tsc1 WT and KO dSPNs, evoked by blue light stimulation of corticostriatal terminals (blue line).

(F) Graph displaying corticostriatal oEPSP amplitude recorded in pairs of Tsc1 WT and KO dSPNs. *p < 0.05, paired t test; n = 9 pairs of neurons from eight mice.

(G) *Tsc1$^{fl/fl}$;D1-tdTomato;Thy1-ChR2-YFP* mice were injected with AAV5-Cre-GFP, and recordings of light-evoked cortically driven action potentials (oAPs) were made from simultaneous pairs of Tsc1 WT and KO dSPNs.

(H) Examples of corticostriatal oAPs recorded over ten trials from a pair of Tsc1 WT and KO dSPNs. Blue line indicates light onset.

(I) Graph displaying the average spike latency per neuron for pairs of simultaneously recorded Tsc1 WT and KO dSPNs. Spike latency was defined as the time in milliseconds from the onset of blue light stimulation to the action potential threshold. *p < 0.05, paired t test.

(J) Graph displaying the spike jitter per neuron for pairs of simultaneously recorded Tsc1 WT and KO dSPNs. Jitter was defined as the SD of the latency to action potential threshold for 4–11 stimulation trials per neuron. For (I) and (J), n = 9 pairs of neurons from nine mice. For (C), (F), (I), and (J), dots indicate the values of individual neurons, and filled circles with error bars indicate the group mean ± SEM for paired recordings. See Table S4 for p values for statistical comparisons.